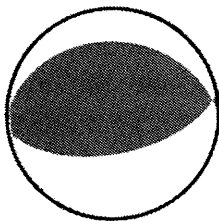


3. Aftershocks and Slip Distribution of Mainshock

3.1 Aftershock Observations

H. Negishi, J. Mori, T. Sato, R.P. Singh and S. Kumar

We planned and installed a temporary array of seismographs to record aftershocks of the 2001 West India earthquake. The main purpose of the aftershock survey was to obtain accurate hypocentral locations so that we could determine the size and orientation of the fault plane that ruptured in the earthquake. From teleseismic data, the focal mechanism showed that the earthquake was a thrust event on a fault that trended roughly in an east-west direction, e.g. Figure 3.1 shows the moment tensor solution determined by Kikuchi and Yamanaka (2001). However, from the teleseismic data it is difficult to resolve which of the nodal planes was the fault plane. The size of the fault plane and distribution of slip were determined by Kikuchi and Yamanaka (2001) and Yagi and Kikuchi (2001) from teleseismic data, although it is difficult to constrain the size of the fault plane only from teleseismic data, as seen from the large variations in these results.



Strike 78 Dip 58 Slip 81

Figure 3.1 Focal mechanisms determined by Kikuchi and Yamanaka (2001).

Instrument Deployment

The Japanese group (Tamao Sato, Hirosaki University, James Mori, Kyoto

University, Hiroaki Negishi, National Research Institute for Earth Science and Disaster Prevention) arrived in Delhi, India on February 25 and met Indian colleagues, Ramesh P. Singh (Indian Institute of Technology, Kanpur), Sushil Kumar, (Wadia Institute for Himalayan Geology), and students from the Indian Institute of Technology. The team of 9 people flew to Ahmedabad on the morning of February 26 and drove to the region of the earthquake that afternoon. We stayed at a Gujarat Police camp in Bhachau for the first few days, during which time 8 portable seismographs were deployed.

Planning the configuration of the array was difficult because of the lack of information on where the aftershocks were occurring. The information we had were mainshock hypocenters reported by the Indian Meteorological Department (IMD), USGS, and IRIS, along with some teleseismic aftershock locations determined by the USGS. We also had moment tensor solutions from Harvard and USGS. There was considerable disagreement between the various epicenters, and teleseismic locations of the aftershocks were spread over a large area and varied in depth from 10 to 100 km. Media coverage of the damage was centered on Bhuj, suggesting that the city was located very close to the fault. This turned out not to be the case and smaller villages east of Bhuj had more severe damage. For a large magnitude earthquake (Mw 7.7, Ms 8.0) we expected the aftershocks to be spread over a large area. However, instead of trying to cover the whole area of the fault with only 8 instruments, we decided to concentrate on one portion of the aftershock distribution with relatively close station spacing, so that we could have good depth control on the events.

For the instrument deployment, we decided to place our stations east of the

3. Aftershocks and Slip Distribution of Mainshock

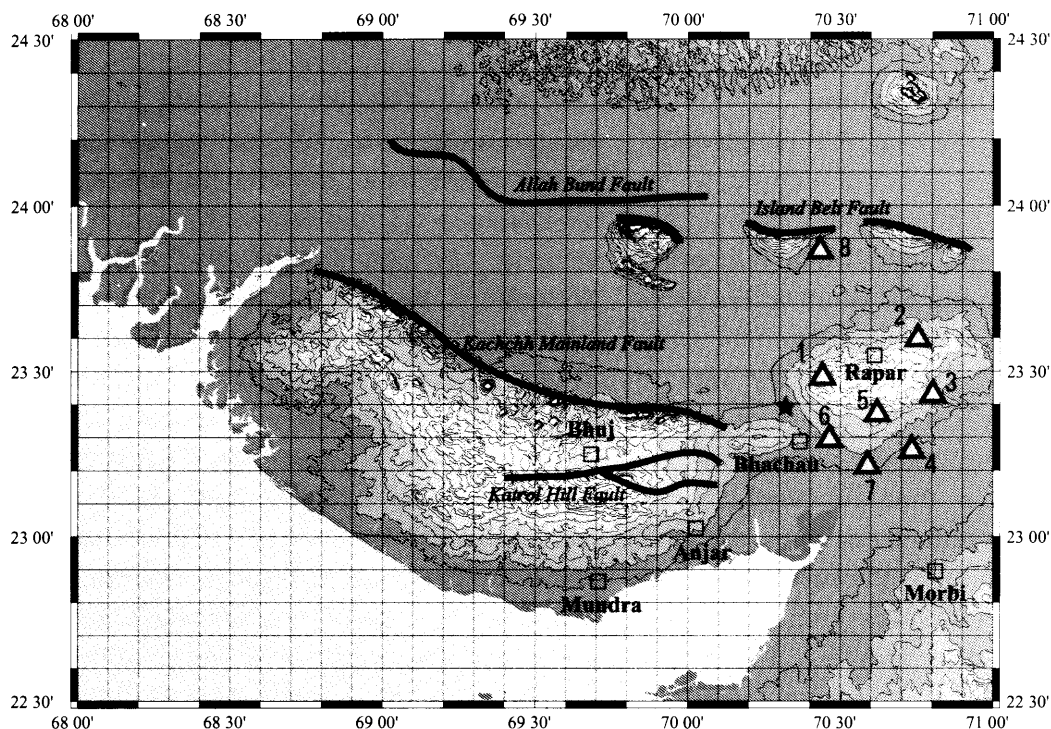


Figure 3.2 Distribution of stations (triangles) used in the aftershock observations. Star is the mainshock epicenter from IRIS. Faults after Malik et al. (2001).



Photo 3.1. Installing instrument on rocky outcrop near Adhoi.

epicenter in an array which extends about 70 km in the north-south direction and 40 km in the east-west direction (Figure 3.2). This decision was based largely on two reasons. First was road accessibility. Much of the region is covered with salt flats (Rann of Kachchh). These areas are inaccessible by

vehicles and would be very bad sites for seismometers. The second reason was some informal information we received from the University of Memphis group. Paul Rydeleck reported that many small aftershocks seemed to be occurring in the eastern part of the aftershock area, although they were not yet able to determine hypocenters.

It was not difficult to find good sites for the seismometers, and about half of the stations were located on or close to rock outcrops (Photo 3.1.). Cultural noise was generally low in the area, although, the instrument at Adhoi was moved a few kilometers on March 1 because it was close to a busy road. All the stations had three-component velocity sensors with natural frequencies of 1 or 2 Hz and 20 bit digital recorders. 5 of the stations were recording continuously and 3 stations recorded triggered data. All of the instruments used sample rates of 100 Hz. Timing was from Global Positioning System (GPS) clocks that

3. Aftershocks and Slip Distribution of Mainshock

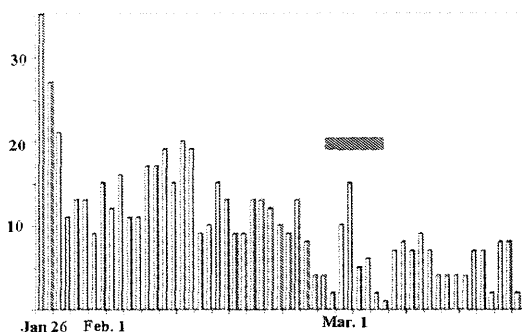


Figure 3.3. Daily frequency of earthquakes recorded by the Indian Meteorological Department (IMD). The bar shows the period of our aftershock observations.

were updated every 6 hours. The details and locations of the instrumentation are shown in Table 3.1 The array of 7 stations (the instrument at Kataria malfunctioned) was in operation for about 7 days from February 28 through March 6.

Although the temporary array deployment was about a month after the mainshock, there was still a considerable number of aftershocks occurring. The IMD national seismic network was recording about 5 to 15 aftershocks per day during the time of our deployment. Figure 3.3 is a plot of the number of aftershocks recorded by the IMD network. In total, we recorded several thousand earthquakes and were able to determine good locations for over 1400 of the larger ($M_{0.5}$ to 3.5) events. The array of

stations we deployed is slightly to the east of the distribution of aftershocks, but it turned out to be close enough so that we were able to obtain good locations.

Aftershock Data and Locations

Figure 3.4 shows a typical example of the three-component waveforms that were recorded for the aftershocks. Generally P arrival times could be picked within about 0.05 seconds and S arrival times within 0.1 to 0.3 seconds. Since there was almost always one station within a distance of the hypocentral depth, there is good control on the depth determinations. Earthquake hypocenters were determined using the JHD program (Engdahl et al., 1982) with a fixed one-dimensional velocity structure and solving for station corrections.

Table 3.2 shows the velocity model which was received from the National Geophysical Research Institute (B.K. Rastogi, pers. Comm.) and used in this study. Table 3.3 lists the station corrections that were determined.

Figure 3.5 shows the epicenters of 1434 aftershocks which were located using the JHD program. P and S arrivals from 5 to 6 stations were used for the locations and RMS time residual ranged from about 0.03 to 0.1 seconds. The star shows the mainshock epicenter as determined by the IRIS. The area of aftershocks, which may be

Table 3.1 Instrument locations and type.

	Station	Latitude	Longitude	Height (m)	Sensor	Recorder
1	Chobari	23.4954	70.3498		Lennartz-1Hz	DAT continuous
2	Rapar	23.6058	70.6429	65	Lennartz-1Hz	DAT continuous
3	Chitrod	23.4489	70.6888	141	Lennartz-1Hz	DAT continuous
4	Kataria	23.2914	70.6239	69	Lennartz-1Hz	DAT continuous
5	Adhoi	23.3735	70.5120	101	L22D- 2Hz	EDR-660 triggered
	Adhoi2	23.3948	70.5183	155	L22D- 2Hz	EDR-660 triggered
6	Bhachau	23.3125	70.3719	51	L22D- 2Hz	EDR-660 triggered
7	Amliyara	23.2455	70.4890	34	L22D- 2Hz	EDR-660 triggered
8	Govindjiva	23.8515	70.3425	62	Lennartz-1Hz	DAT continuous

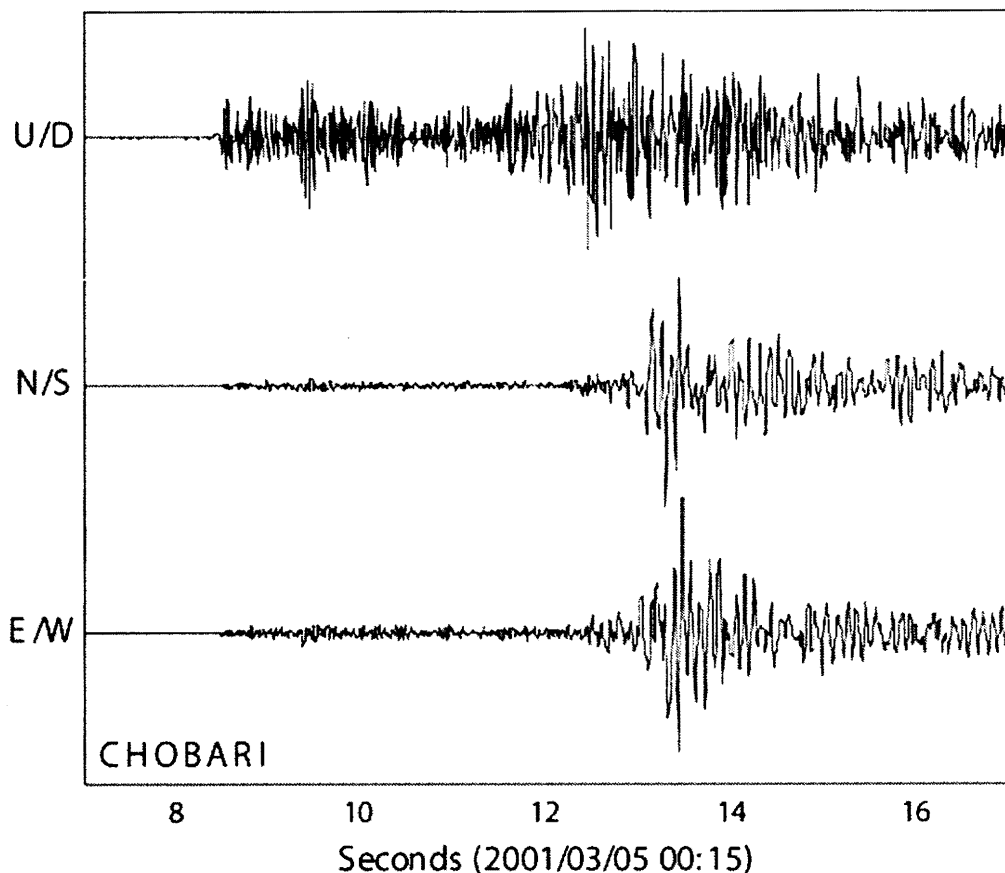


Figure 3.4. Example of waveform recorded at Chobari station for M1.9 earthquake located 41km from the station.

interpreted as the area of the fault that ruptured during the mainshock has dimensions of about $40 \times 40 \text{ km}^2$, extending from about 23.3° N to 23.7° N in the north-south direction and 70.1° E to 70.5° E in the east-west direction. There is the possibility that the station distribution may bias our estimate of the size of the aftershock area. With most of the stations to the east, there may be more events toward the west that are not located by our network. However, the aftershock area determined by the Univ. of Memphis (2001) is very similar to our results. Their network extended more evenly over a larger region that included Bhuj. Their epicenters tend to show more events for the western portion of the aftershock zone, but the overall size of the aftershock area is similar to our results. Our distribution of

aftershocks also shows a region with relatively few events in the area around the mainshock epicenter and a large cluster of events to the east.

Figure 3.5 shows cross sections of the hypocenters which are oriented in directions along and perpendicular to the $\text{N}78^\circ \text{ E}$ direction. This is the strike direction of one of the nodal planes of the moment tensor solution from Kikuchi and Yamanaka (2001). The direction was chosen because it produces the clearest alignment of hypocenters on a southward dipping trend in the cross section perpendicular to the fault.

Projections of the aftershocks on other directions within a range of about $\pm 15^\circ$ does not change the distribution significantly and the pattern of events still shows the southwest-dipping trend. In the two cross

3. Aftershocks and Slip Distribution of Mainshock

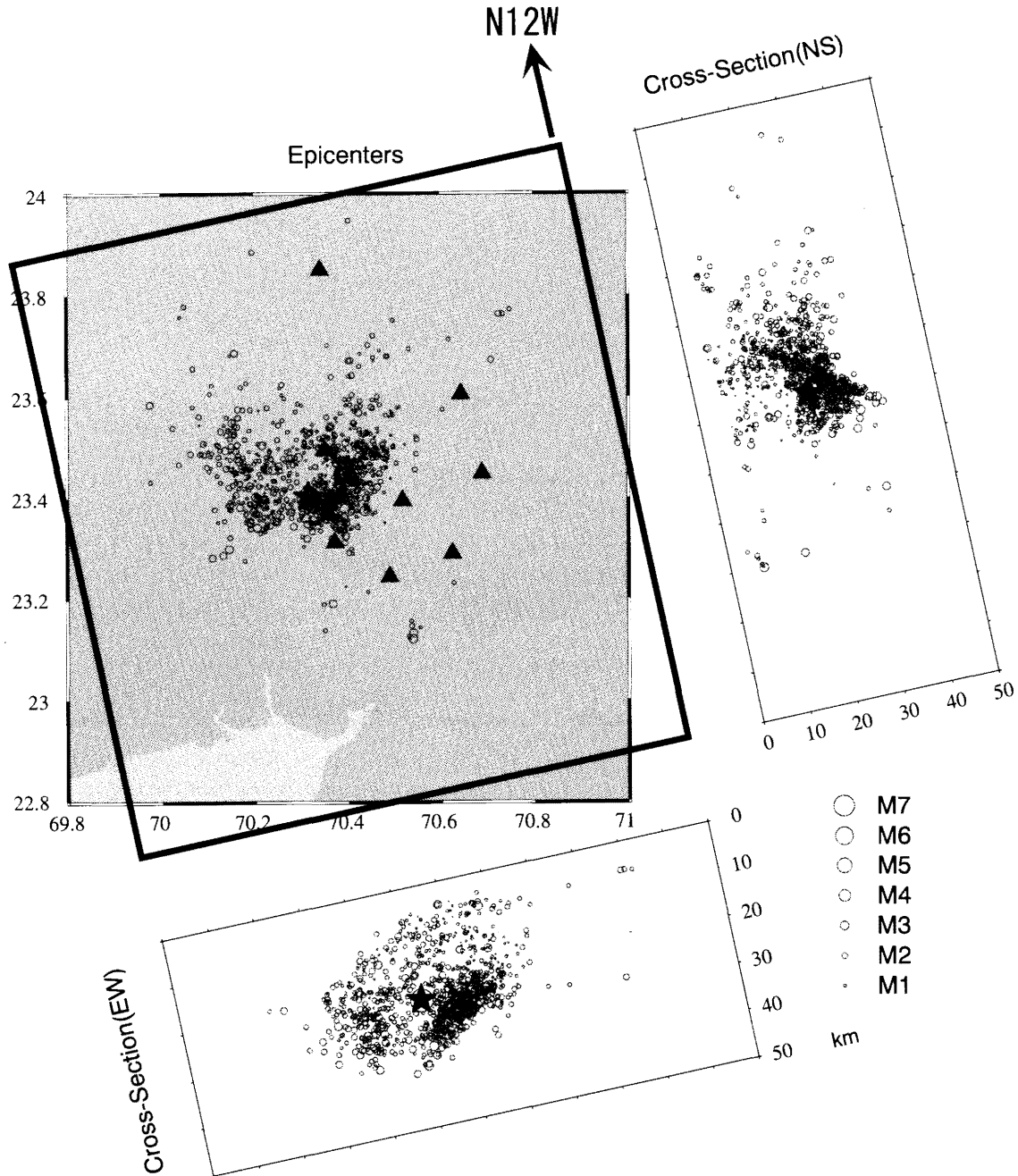


Figure 3.5. Aftershock locations determined in this study. Cross section on right is perpendicular to the fault strike. Cross section below is along the fault. Star is the mainshock epicenter.

sections, the depth range of aftershocks is from about 10 to 35 km. The distribution of aftershocks does not appear to come very close to the surface. In the cross section perpendicular to the fault, one sees a trend in the data that dips generally toward the south, but there are many events that are off this trend. We think that these locations are

correct and that there are many aftershocks that occurred away from the fault plane.

Relationship of Aftershocks to Mainshock Fault

Our locations of aftershocks indicate a plane that dips toward the south at about 45 degrees. We interpret this feature as the

3. Aftershocks and Slip Distribution of Mainshock

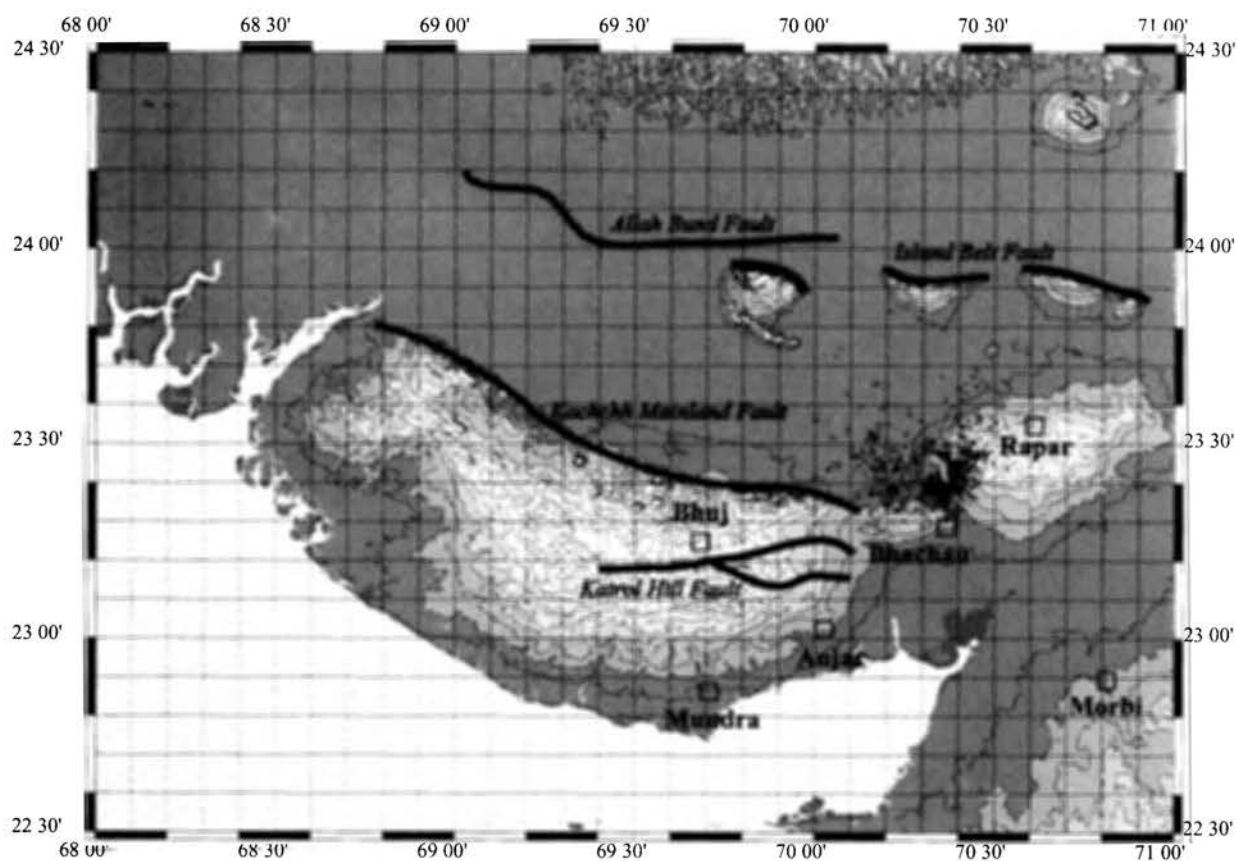


Figure 3.6. Aftershocks located in this study and their relation to the mapped faults of the region. Faults after Malik et al. (2001).

Table 3.2 Velocity model used to locate earthquakes.

Depth (km)	P velocity (km/sec)	S velocity (km/sec)
0.2	4.99	2.88
0.3	3.40	1.96
2.9	4.70	2.72
3.0	5.76	3.33
6.0	6.21	3.59
20.5	7.01	4.05
30.0	6.66	3.85
37.0	8.47	4.90

Table 3.3. Station corrections calculated from JHD program

Station	P corr. (sec)	S corr (sec)
Chobari	0.080	-0.090
Rapar	0.085	-0.193
Adhoi	-0.017	-0.165
Adhoi2	-0.044	-0.308
Amliyara	0.082	0.034
Govindjiva	-0.021	-0.287
Bhachau	0.007	-0.095

fault plane of the mainshock. The surface projection of this plane does not match any of the mapped faults in the area. The aftershocks are east and north of the Kachchh Mainland fault and south of the Allah Bund-Island Belt Faults (Figure 3.6). The aftershocks and mainshock focal mechanism indicate a fault that strikes in

east or east-northeast direction with a surface projection that is near the southern edge of the Rann of Kachchh, west of the town of Rapar. There are no obvious geological or topographic indications of a causative fault in this area, though we find many cracks and fissures that seem to have been produced by the strong ground

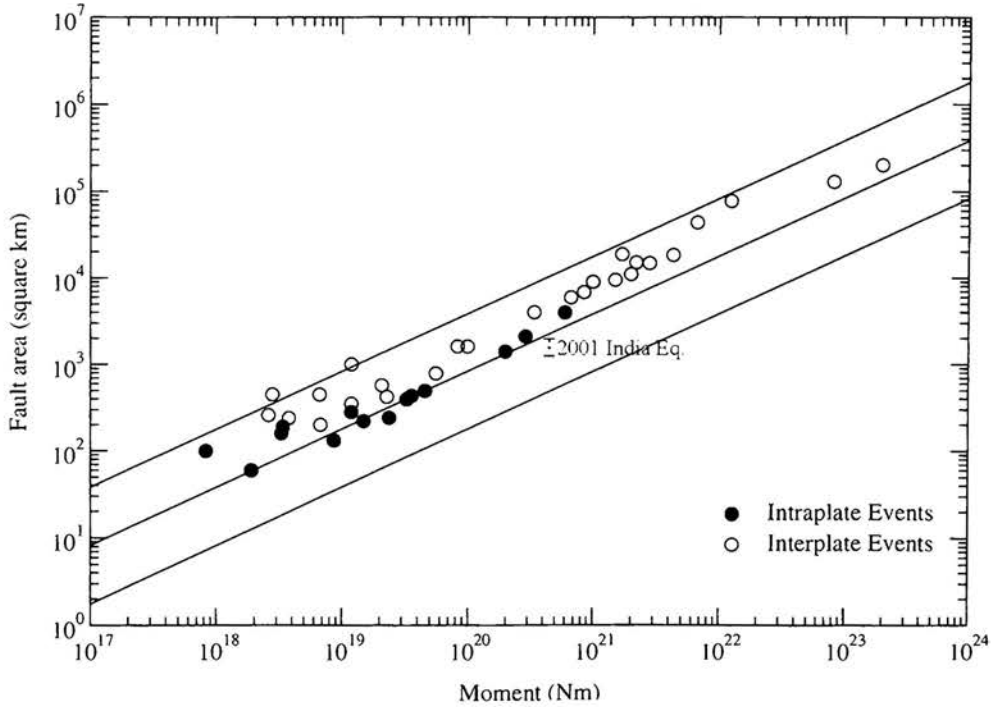


Figure 3.7. Relation between fault area and moment taken from Kanamori and Anderson (1975).

shaking.

In the map view and cross section along the fault, that is projected along the fault, there is an area of relatively few aftershocks in the region surrounding the mainshock hypocenter. This area near the hypocenter is also where largest amount of slip occurred during the earthquake (see Section 3.2 on Slip Distribution of Mainshock). This is similar to observations in other earthquakes which show aftershocks distributions that tend to cluster around the edges of large asperities (Mendoza and Hartzell, 1988)

Mainshock Source Size

The overall dimension of the aftershock distribution is small for a Mw 7.7 earthquake. For example, the 1999 Chichi earthquake (Mw7.7), Taiwan, had an aftershock area of about $40 \times 100 \text{ km}^2$ (Hirata et al., 2000) which is more than twice the size of the West India earthquake aftershock area. The small area implies that

the static stress drop is high. If we assume that the region of the aftershocks is comparable to the area of the fault, the area has a radius (r) of 20 to 25 km. Using the formula for a circular fault (Eshelby, 1957)

$$\Delta\sigma = 7/16 * M_0/r^3$$

the static stress drop is 12.6 to 24.6 MPa (126 to 246 bars) for a moment of $4.5 \times 10^{20} \text{ Nm}$. This is a rather high value for a large earthquake. Intraplate earthquakes tend to have higher static stress drops than interplate earthquakes (Kanamori and Anderson, 1975), but this stress drop is high even among intraplate events. Figure 3.7 shows the relation of fault area as a function of seismic moment from Kanamori and Anderson. The 2001 India event has one of the higher static stress drop for the earthquakes in their data set.

As of May 1, the largest aftershock (mb5.9, USGS) occurred 2 days after the mainshock. The size of this aftershock is

small compared to the mainshock, so, fortunately, there was no serious secondary damage reported. Also there are no reports of foreshocks prior to this earthquake. According to the USGS/NEIC catalogue of regional seismicity, since 1973 the only significant earthquake to occur within the region of Figure 3.5, was a mb4.8 event (23.34°N, 70.61°E, depth 33km) on July 18, 1982.

Conclusions

We installed a temporary array of seismographs in the region of the 2001 West India earthquake which was operating from February 28 through March 6. We located over 1400 aftershocks. The distribution of aftershocks showed the following features.

1. The aftershocks showed a plane that dips toward the south at about 45°. This is interpreted as the fault plane of the mainshock.
2. The depth distribution of events is from about 10 to 35 km. The aftershocks do not appear to extend to the surface.
3. The aftershocks cover an area of about 40 x 40 km². This is small for a Mw7.7 earthquake and implies a high static stress drop of 12.6 to 24.6 MPa.

It was surprising that a shallow earthquake of this size that caused a large number of casualties (over 20,000) and severe damage did not have surface faulting. This is explained by our aftershock results which show that the fault plane of this event was slightly deeper than many large damaging earthquakes, extending from about 10 to 35 km depth. This result is important for future evaluations of seismic hazards in continental areas. Large damaging earthquakes can occur without leaving evidence of surface faulting. Furthermore, large earthquakes can occur on buried faults which show no displacement or topographic

features at the surface.

References

- Engdahl, E.R., J.W. Dewey, and K. Fujita, (1982). Earthquake location in island arcs, *Phys. Earth Planet. Inter.* **30**, 145-156.
- Eshelby, J.D. (1957). The determination of the elastic field of an ellipsoidal inclusion and related problems, *Proc. Roy. Soc. London, Series A*, **241**, 376-396.
- Hirata, N., S. Sakai, Z-S Liaw, S-B Tsai, S-B Yu (2000) Aftershock observation of the 1999 Chi-Chi, Taiwan, earthquake, EOS, *Transactions, Amer. Geophys. Union*, **81**, F875.
- Kanamori, H. and D.L. Anderson (1975). Theoretical basis of some empirical relations in Seismology, *Bull. Seismol. Soc. Am.*, **65**, 1073-1095.
- Kikuchi, M and Y. Yamanaka (2001). Western India earthquake, <http://www.eic.eri.u-tokyo.ac.jp/index-e.html>.
- Malik, J.N., P.S. Sohoni, S.S. Merh, R.V. Karanth (2000). Paleoseismology and neotectonics of Kachchh, Western India, Active Fault Research of the New Millenium, *Proceedings of the Hokudan International Symposium and School on Active Faulting*, Okumura, K, H. Goto, K. Takada, eds., 251-259.
- Mendoza, C. and S.H. Hartzell (1988). Aftershock patterns and main shock faulting, *Bull. Seismol. Soc. Am.*, **78**, 1438-1449.
- University of Memphis (2001). Gujarat epicenters and temporary station locations, <http://www.ceri.memphis.edu/~withers/Gujarat/>.
- Yagi, Y. and M. Kikuchi (2001). Western India earthquake, <http://www.eic.eri.u-tokyo.ac.jp/index-e.html>.

3. Aftershocks and Slip Distribution of Mainshock

we use a fault grid that covers an area of 50 x 40 km². It would be unusual for a shallow earthquake if the extent of mainshock faulting were significantly larger than the area of aftershocks. In almost every case, the area of aftershocks is larger than the area of inferred fault slip. The grid used in this study has 80 (10 x 8) subfaults spaced at 5 km intervals (Figure 3.9).

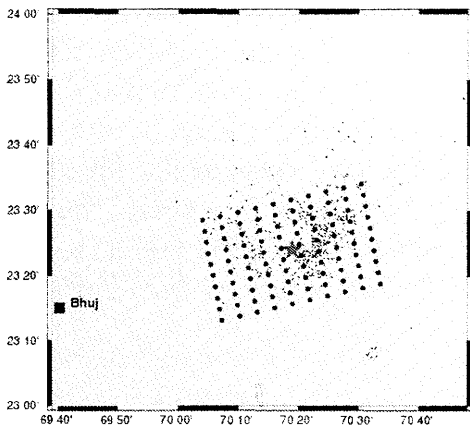


Figure 3.9. Grid used for inversion for teleseismic data.

Slip Distribution

The results of the inversion for the various rupture velocities tested, did not show significant differences. In Figure 3.10, we show the results for a rupture velocity of 2.9 km/sec, which corresponds to 0.78 times the local shear-wave velocity. The results of the inversion show that the largest area of slip is close to the hypocenter. This asperity is about 10 x 20 km² with a maximum slip of about 10 meters. The rupture appears to have spread from the hypocenter in a mostly symmetric pattern, with slightly more slip toward the west.

There were several slip distribution solutions done by Kikuchi and Yamanaka (2001) and Yagi and Kikuchi (2001). Our solution is rather similar to the model of Kikuchi and Yamanaka, although the fault area of our model is slightly smaller. The

other solutions by Yagi and Kikuchi (2001) show significantly larger fault areas than our slip distribution.

The fit of the model waveforms and the observed data are shown in Figure 3.11. Looking at the observed waveforms, we can see some features that are consistent with the results of our slip distribution model. The waveforms of the observed data look generally similar at all azimuths, indicating a rather symmetric rupture, as seen in our model. Also, the waveforms are all quite impulsive with the largest amplitudes in the first pulse. This is an indication that the largest slip occurred at the beginning of the rupture, in the region close to the hypocenter.

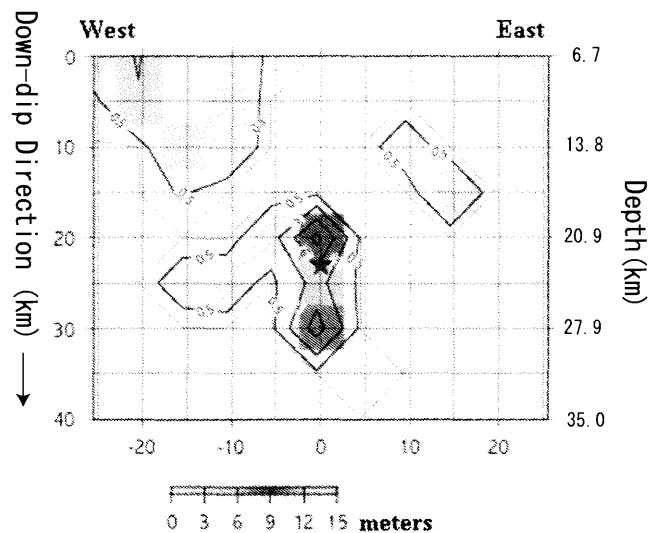


Figure 3.10. Distribution of slip on the fault assuming a rupture velocity of 2.9 km/s.

The character of the slip distribution is different from other shallow earthquakes of equal size. As noted in the section on aftershock observations, the area of the fault is small for a Mw7.7 event. We can see the differences in Figure 3.12, which compares the slip distribution of the 2001 West India

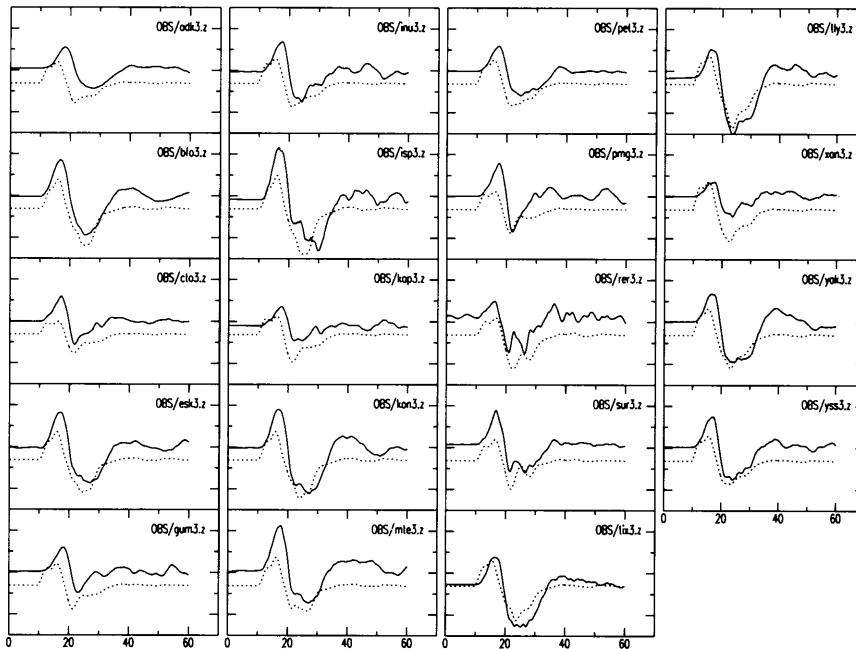


Figure 3.11. Comparison of observed P waves (solid lines) and calculated synthetic seismograms (dotted lines) for our slip distribution model.

earthquake to the similarly sized (Mw7.7) 1999 Chichi, Taiwan earthquake (Ma et al., 2001). The Taiwan earthquake is spread out over a larger area and shows a more complicated slip distribution. The difference can also be seen in the teleseismic waveforms. Figure 3.13 shows a comparison of P waves for the two events with the same amplitude and time scales. The India event has a more compact waveform with a large amplitude pulse at the beginning. The Taiwan data shows a more complicated waveform with overall longer duration and smaller amplitudes. The area of large slip in the region of the hypocenter corresponds closely to the area of most severe damage in the villages east of Bhuj (see Section 6.1.). This area probably experienced very strong shaking from the rupture of the asperity. Bhuj is located more than 30 km from the closest portion of the fault and probably experienced somewhat lower levels of ground motions, as seen in the intensity distribution.

If the features of the teleseismic waveforms can be extrapolated to the near-field ground motions, the strong-ground motions started with a large coherent pulse from the asperity that would have produced large ground velocities and displacements. Comparison of the teleseismic data with the 1999 Chichi, Taiwan earthquake suggests that the 2001 West India earthquake may have produced very strong long-period velocities and displacements in the near-field that were larger than other shallow earthquakes of similar size. Compared to other shallow earthquakes of the same moment, the slip occurred over a smaller area (higher static stress drop) and in a shorter amount of time. As mentioned in the section on aftershock observations, the relatively small fault area gives a high static stress drop of 16 MPa. One modifying point in inferring the strong motions for this earthquake from our modeling, is that the fault is slightly deeper than other shallow earthquakes, so that the closest distances to the fault are

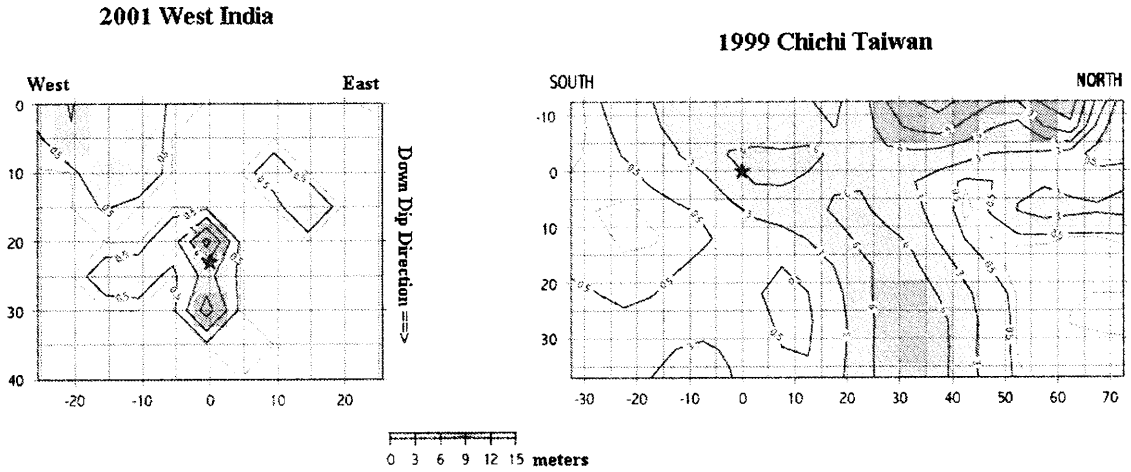
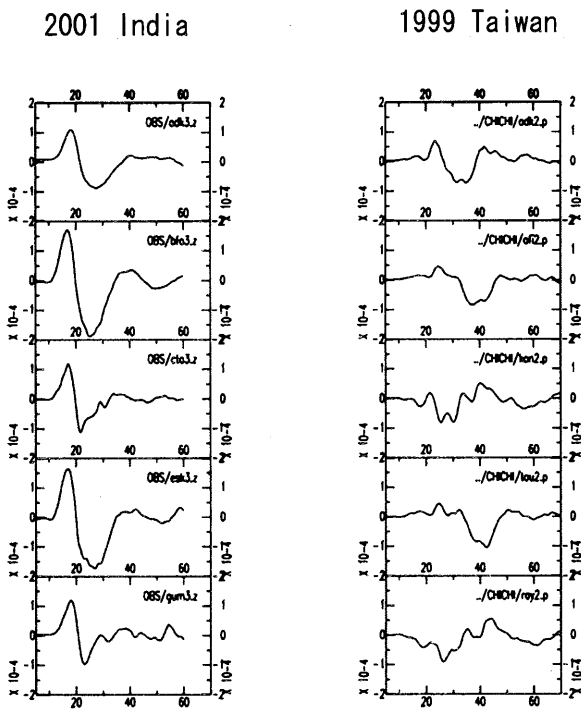


Figure 3.12. Comparison of slip distribution for the 2001 West India and 1999 Chichi Taiwan.



Figures 3.13. Comparison of teleseismic P wave for the 2001 India and 1999 Chichi, Taiwan earthquake.

slightly larger than for other shallow earthquakes. Unfortunately, there are no nearfield strong-motion records of the India earthquake to verify our conclusions.

Conclusions

We used the results from the aftershock observations to constrain the size and orientation of the mainshock fault. Using this geometry, we carried out a finite-fault slip inversion using teleseismic P-wave data. The results show an area of large slip in the region of the hypocenter. Compared to other similar size events, such as the 1999 Chichi, Taiwan earthquake, the 2001 West India earthquake ruptured a smaller fault area and had a simpler slip distribution. The teleseismic data show a large initial pulse that is interpreted as the rupture of large asperity near the hypocenter. This pulse may have caused the ground velocities and displacements in the region of the epicenter that were larger than other similar sized shallow earthquakes.

References

Hartzell, S. and T.H. Heaton (1983). Inversion of strong ground motion and teleseismic waveform data for the fault rupture history of the 1979 Imperial Valley, California earthquake, *Bull. Seismol. Soc. Am.*, **73**, 1553-1583.
 Kikuchi, M and Y. Yamanaka (2001). Western India earthquake,

3. Aftershocks and Slip Distribution of Mainshock

<http://www.eri.u-tokyo.ac.jp/index-e.html>.

- Langston, C. A. and D.V. Helmberger (1975). A procedure for modeling shallow dislocation source, *Geophys. J.* **42**, 117-130.
- Ma, K.-F., J. Mori, S-J Lee, S.B. Yu (2001). Spatial and temporal distribution of slip for the 1999 Chi-Chi, Taiwan earthquake, *Bull. Seismol. Soc. Am* (in press).
- Yagi, Y. and M. Kikuchi (2001). Western India earthquake, <http://www.eri.u-tokyo.ac.jp/index-e.html>.

4. Postseismic Crustal Deformation
Deduced from GPS Observations

Miyashita, K., K. Vijaykumar, T. Kato, Y. Aoki and C. D. Reddy

4.1 Introduction

It has been reported that the Gujarat, India earthquake (Ms7.9) of January 26, 2001 caused really the worst damage (20,005 fatalities, 166,000 wounded and 370,00 razed houses) in the India's recorded history. This earthquake was a major intraplate event in the Indian sub-continental plate, which is moving in the north-northeastern direction to collide with the Eurasian plate (Bilham and Gaur, 2000). The hypocenter has been determined at 23.40°N, 70.32°E, and depth of 23.6 km (IRIS, 2001). The Kachchh peninsula including the epicenter has been classified as a very high-risk zone with a possibility of severe damage. The Seismological Observations of Indian Meteorological Department have classified this region as one of the most seismically active zones (Zone-V) (Arya, 2000). There have occurred several large earthquakes in this region, among which the 1819 event with M8 has been extensively studied (Bilham, 1999).

It is very important to investigate the mechanisms for preseismic, coseismic and postseismic crustal deformations in order to understand the complete processes of the major intraplate earthquake. The high precision GPS observations in combination with earlier geodetic observations could possibly detect and map the crustal deformations that are lasting before and after the major event. In such a view, we have started GPS observations around the source region to detect the postseismic crustal deformation and investigate its mechanism. We will report here a preliminary result obtained from two

campaigns of our GPS observations.

4.2 GPS observations

It has been possible to estimate coordinates of observation stations within 1 cm from GPS data, obtained from an appropriate network with dual-frequency GPS receivers. Therefore, we could detect a postseismic crustal deformation, based on the GPS data from repeated observations with the same network.

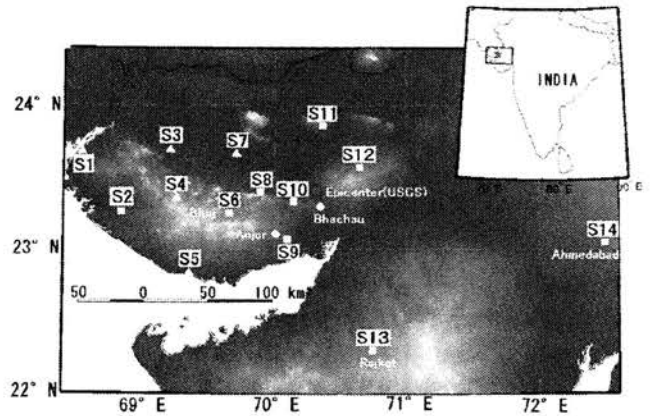


Figure 4.1 GPS network consisting of 14 re-observable stations (S1, ..., S14). Red star denotes the epicenter determined by USGS.



Photo 4.1 GPS antenna installed on a roof-top of the building (in Lodai (S8)), which was not collapsed by the earthquake. The background shows completely destroyed houses.

Figure 4.1 shows a temporary GPS network, which was established two weeks after the earthquake occurrence. The network consisted of 14 observation stations, where GPS antennae were mostly set up on roof-tops of the buildings, which were not destroyed by the earthquake (e.g., Photo 4.1). The average station interval of the network was around 25 km. Coordinates of the stations and types of the dual-frequency GPS receivers used are listed in Table 4.1.

Table 4.1 Coordinates of observation sites and types of GPS receivers

Name	Latitude	Longitude	Receiver
N.Sarovar(S1)	23.6766N	68.5408E	Leica
Naliya(S2)	23.2571N	68.8352E	Trimble
Hajipir(S3)	23.6897N	69.2073E	Leica
Nakhatrana(S4)	23.3555N	69.2549E	Leica
Mandvi(S5)	22.8335N	69.3541E	Leica
Bhuj(S6)	23.2542N	69.6540E	Trimble
Bhirandiyar(S7)	23.6616N	69.7068E	Leica
Lodai(S8)	23.3937N	69.8916E	Trimble
Gandhidham(S9)	23.0694N	70.0951E	Trimble
Dhamdkapir(S10)	23.3317N	70.1430E	Trimble
Ratanpar(S11)	23.8597N	70.3634E	Trimble
Rapar(S12)	23.5682N	70.6435E	Trimble
Rajkot(S13)	22.2923N	70.7740E	Trimble
Ahmedabad(S14)	23.0443N	72.4946E	Trimble

The first campaign of GPS observations was held during a period from February 22 to March 5, and the second campaign during a period from May 13 to May 23. We made 24-hour observations with a sampling rate of 30 sec and an elevation mask of 15 degrees.

4.3 Coseismic crustal deformation

We have not yet obtained the data about the coseismic crustal deformation. However, we could get some information of the earthquake fault from the results of body wave inversion (Yagi and Kikuchi, 2001) and aftershock distribution (this issue). According to these studies, we depicted a

preliminary model of the earthquake fault as follows: coordinate of the upper left corner (23.4°N, 70.0°E); depth of the upper strike 10 km; length 66 km; width 35 km; dip-angle 45°; strike-direction N78°E; slip angle 81°; slip amount 4.18 m. Figure 4.2 shows the distributions of (a) vertical and (b) horizontal surface displacements in and around the source region, calculated for the expected reverse fault model.

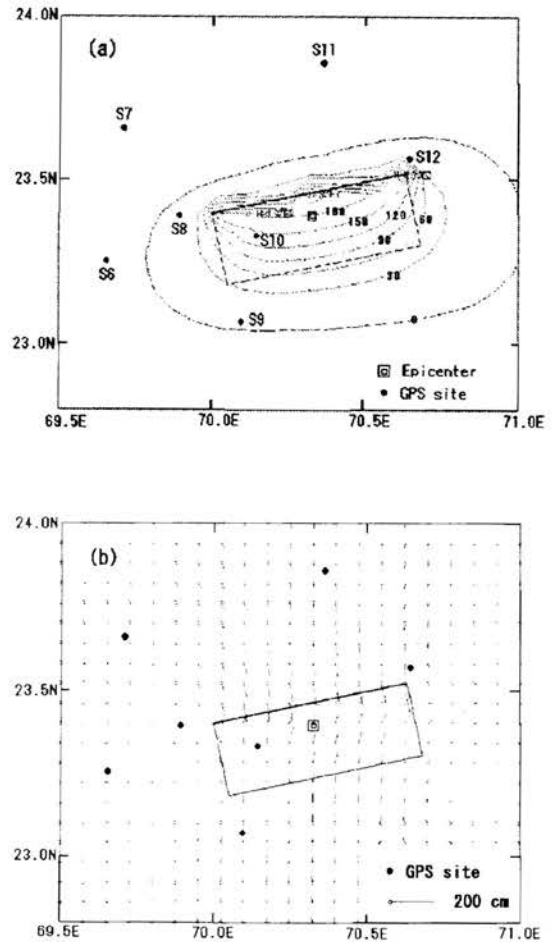


Figure 4.2 Distributions of (a) vertical and (b) horizontal surface displacements due to the preliminary fault model. Contour interval is set up to be 30 cm. Large rectangle indicates a surface projection of the fault model, and a small double-square the earthquake epicenter.

According to the model, the maximum uplift amounted to 243 cm, and the

maximum horizontal displacement 165 cm. We could also expect from the model that the baseline vector between S11 and S12 (Fig. 4.1) changed as follows: its E-W, N-S and U-D components increased -1.29, -18.8 and 23.4 cm, respectively, i.e., $\Delta b_{S11S12} = (-1.29 \ -18.8 \ 23.4)$. We also estimated that $\Delta b_{S11S6} = (-5.91 \ 30.7 \ 2.18)$ and $\Delta b_{S6S12} = (4.62 \ -49.5 \ 21.2)$. It should be noticed that the GPS sites of S6 and S12 were located on the hanging-wall side of the fault plane, but S11 on the foot-wall side. We will discuss about the coseismic and postseismic surface displacements, using these changes of baseline vectors.

4.4 Postseismic crustal deformation

We analyzed the GPS data from the first and the second campaign of GPS observations by using a combination of the GAMIT and the GLOBK software (King and Bock, 1998; Herring, 1998). We also used the data from the fiducial stations of International GPS Service for Geodynamics (IGS) around the network, i.e., Lhasa, Kitab, Diego, Bangalore, Bahrain and Shanghai. These IGS stations were constrained to vary within 3~5 mm horizontally and 5~10 mm vertically from their a priori coordinate values in the ITRF96 reference frame. Baseline solutions for each of the campaigns were obtained by combining daily solutions.

Figure 4.3 shows the changes in the north-south (N-S), east-west (E-W) and up-down (U-D) components of the baseline vectors, b_{S11S12} and b_{S6S12} (Fig. 4.1) near the source region during a period between the two campaigns. It can be seen that the site of S12 on the hanging-wall side of the expected fault plane was uplifted about 2.8 cm with respect to S11 on the foot-wall side during a postseismic interval of about 80 days. The amount of uplift was larger than 10 % of the coseismic one. It was indicated

from the present baseline analysis that $\Delta b_{S11S12} = (-0.36 \ 0.12 \ 2.8)$, $\Delta b_{S11S6} = (-0.55 \ 0.21 \ 1.6)$ and $\Delta b_{S6S12} = (0.19 \ -0.09 \ 1.3)$. We could find that the postseismic changes of U-D components were larger than those of N-S and E-W components. Concerning the baseline vectors around the source region, it could also be noticed that the postseismic deformation patterns were similar to the coseismic ones, calculated from the expected fault model, in spite of smaller changes in their magnitudes.

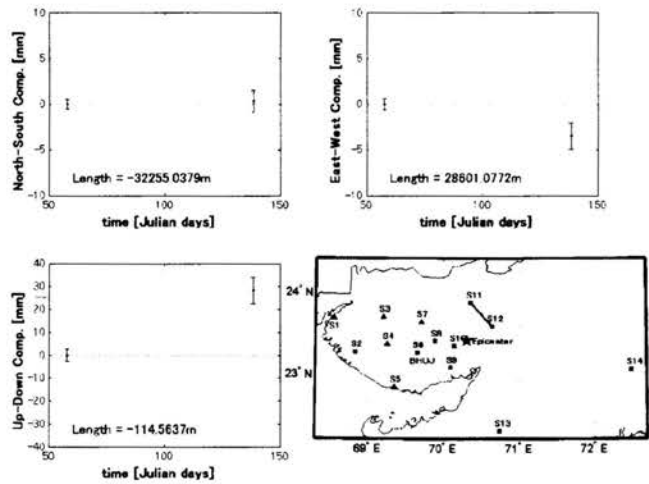


Figure 4.3(a) Changes of N-S, E-W and U-D components of the baseline vector, b_{S11S12} .

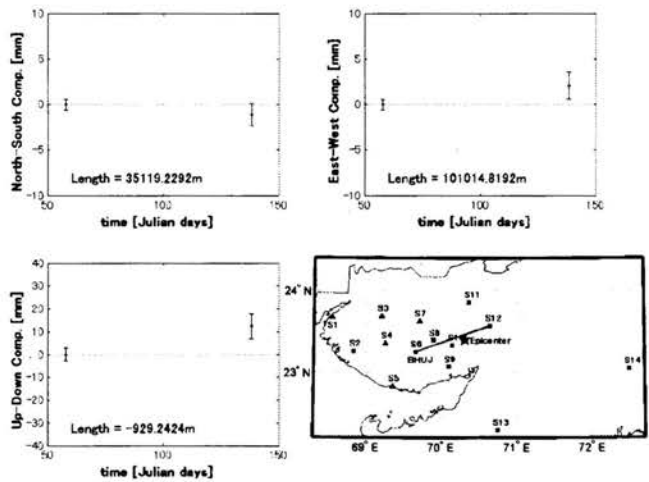


Figure 4.3(b) Changes of N-S, E-W and U-D components of the baseline vector, b_{S6S12} .

4.5 Discussion and conclusion

We could detect the postseismic crustal deformation associated with the 2001 Gujarat earthquake from the two campaigns of GPS network observations. The baseline solutions for the GPS data indicated that the changes of vertical components were prominent, and the postseismic deformation patterns were similar to the postulated coseismic ones.

Postseismic deformation studies are essential to understanding the process of strain accumulation and release in a seismogenic region, which is in turn fundamental to understanding earthquake recurrence processes. The possible mechanisms for postseismic deformations have been studied in terms of (1) aseismic slip on a coseismic fault plane and/or on its extensional plane, and (2) viscoelastic relaxation associated with an earthquake faulting (e.g., Scholz and Kato, 1978; Miyashita, 1987; Savage and Thatcher, 1992; Savage et al., 1994).

We have not yet clearly depicted the mechanism for the present postseismic crustal deformation. However, it is expected that aseismic slip on the coseismic fault plane and/or on its upward extension may be responsible for the present postseismic crustal deformation. It is because the postseismic deformation patterns for the baseline vectors around the source region were similar to the coseismic ones predicted as shown previously, and the upper edge of the coseismic fault plane was located at a depth of about 10 km. However, it should be a temporary summary, until the precise coseismic fault plane is estimated.

Finally, we indicate some of the on-site earthquake-related damages and phenomena in and around the source region, which were observed during the first GPS campaign.

We found total destructions in the residential localities, where many of the houses were constructed with stone masonry and mud mortar (Photo 4.2).



Photo 4.2 Completely destroyed houses with stone masonry and mud mortar.

Widespread liquefaction sites were observed in the regions with low altitudes, where the lands are usually dry except in the rainy season (Photo 4.3).



Photo 4.3 Liquefaction site. Overflowed salt water was seen around the aquifer spring.

Although no surface faulting was observed in and around the source region, a large surface crack with a length of about 300~400 m, which might be caused by strong ground motion and land-sliding, was found along a manmade reservoir (Photo 4.4).



Photo 4.4 Bird's eye view of a large surface crack with a length of about 350 m, whose left portion slid down partially to the lake-side.

References

- Arya, A. S. (2000). Recent developments toward earthquake risk reduction in India, *Current Science*, 79, 1270-1277.
- Bilham, R., and V. K. Gaur (2000). Geodetic contribution to the study of seismotectonics in India, *Current Science*, 79, 1259-1268.
- Bilham, R. (1999). Slip parameters for the Rann of Kachchh, India, 16 June 1819 earthquake, quantified from contemporary accounts, *Geological Society London*, 146, 295-318.
- Herring, T. A. (1998). GLOBK: Global Kalman filter VLBI and GPS analysis program version 4.1, *Massachusetts Institute of Technology, Cambridge*.
- IRIS. (2001). Special Event Page January 26, 2001 Western India, 7.7 Mw* <http://www.iris.washington.edu/DOCS/sindia.htm>
- King, R. W., and Y. Bock (1998). Documentation for GAMIT GPS analysis software, *Massachusetts Institute of Technology, Cambridge and University of California at San Diego*.
- Miyashita, K. (1987). A model of plate convergence in southwest Japan, inferred from leveling data associated with the 1946 Nankaido earthquake, *J. Phys. Earth*, 35, 449-467.
- Savage, J. C., M. Lisowski, and J. Svarc (1994). Postseismic deformation following the 1989 (M=7.1) Loma Prieta, CA, earthquake, *J. Geophys. Res.*, 99, 13757-13765.
- Savage, J. C and W. Thatcher (1992). Interseismic deformation at the Nankai Trough, Japan, subduction zone, *J. Geophys. Res.*, 97, 1117-1135.
- Scholz, C. H., and T. Kato (1978). The behaviour of a convergent plate boundary: Crustal deformation in the South Kanto district, Japan, *J. Geophys. Res.*, 83, 783-797.
- Yagi, Y. and M. Kikuchi (2001). Results of Rupture Process for January 26, 2001 Western India Earthquake (Ms 7.9), <http://www.eic.eri.u-tokyo.ac.jp/yuji/southindia/index.html>

5. Outline of Damage Survey

H. Murakami

(1) Introduction

According to the report by the Crisis Management Center of Indian Government (Ref. 1), extent of human loss is enormous with 20,005 human lives lost, 166,000 people injured (among which 20,717 seriously injured), and 247 people missing (as of 2001.03.20). Number of dwelling damage is indicated in Table 1. Fully destroyed dwellings reached 370 thousand units, and partially destroyed dwellings reached 922 thousand units. This earthquake disaster in Gujarat, India is comparable and even worse than the 1999 Kocaeli, Turkey earthquake, in which 15,466 people lost their lives, 60 thousand dwelling units were collapsed or heavily damaged, and 59 thousand dwelling units were moderately damaged (Ref. 2). In the 1995 Hanshin-Awaji earthquake, 6,400 people lost their lives and 181 thousand dwellings were collapsed or heavily damaged.

Table 5.1. Number of dwelling damage in the 2001 Bhuj earthquake

	Pucca permanent	Kachcha temporal	Huts	Total
Fully destroyed	187	167	16	370
Partially destroyed	501	387	34	922
Total	688	554	50	1292

Ref.: Gov. of India, Krishi Control Room, 20 Mar 2001 report
<http://www.ndmindia.nic.in> Unit = thousand

Using the database of significantly damaging earthquakes in the world by Utsu (Ref. 3), earthquakes in India from 1800 thru 2001 with human loss exceeding 100 are searched and relation of earthquake magnitude (Richter's scale M) and human loss are depicted in Fig. 1. Normal correlation between the magnitude and human loss can be observed, and the 2001

Gujarat earthquake is one of the most deadliest event thru the last 200 years.

Table 2 indicates fundamental statistics in the State of Gujarat. Its population of 41,310,000 is almost a third of the total in Japan, and the land area of 197 thousand sq.km is almost a half of that in Japan. Population density is 211 persons/sq.km. The rate of population increase is very steep (Fig. 2), and very high percentage of 21% increase was recorded between 1981 and 1991. Such rapid population growth certainly may have an effect on low building standard and poor enforcement of seismic safety regulations.

Earthquakes in India (1800-2001, Dead>100) by Utsu Database 2001Gujarat eq

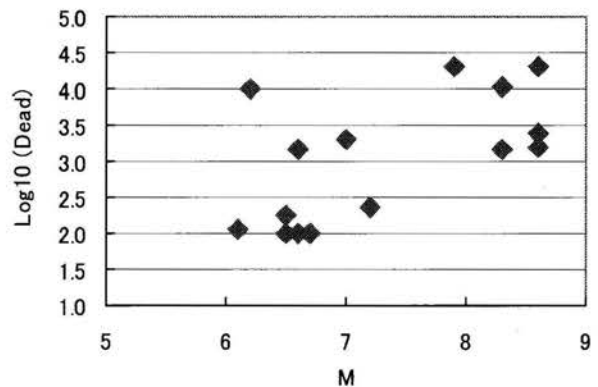


Figure 5.1. Earthquake magnitude and total number of fatality.

Table 5.2. Statistics for the Gujarat state

State Capital	Gandhi Nagar
Population ('000s in 1991)	41,310
Area ('000 sq. km)	196
Females per 1000 males (1991)	934
Literacy rate (1991)	61.3
Ratio of urban population (1991)	34.5
Net Domestic Product (Rs. million at current prices in 1992-	322,400
Per Capita Income (Rs. at current prices in 1992-93)	7,586
Principal Language	Gujarati
Population density (person/sq.km)	211

5. Outline of Damage Survey

(2) Distribution of human loss and dwelling damage

Table 3 indicates number of human loss and population for the districts in the state of Gujarat. In Kachchh district alone, 92% of total human loss (18,416 out of total 20,005) occurred. In the city of Ahmedabad, which is a economic center of Ahmedabad district (population 5.8 million), approximately 60 mid or low rise apartment buildings and 3 high rise apartment buildings collapsed and 750 residents lost their lives.

Taluka-wise damage statistics of the Kachchh district are indicated in Table 4. Taluka is an administrative division of each district. In addition to the damage to Reinforced Concrete buildings, traditional type of dwellings such as Pucca (permanent dwellings made of brick or stone masonry) and Kachcha (temporal dwellings made of mud wall and straw roofs). Fig. 3 indicates distribution of human loss ratio (%) of each taluka division. Bhachau taluka (Bhachau center and surrounding villages), located within 12km of epicentral distance, suffered highest ratio of human loss amounting to 6.47%. Number of human loss in Bhachau taluka reached 7,424 and shared a third of the total. Ratio of collapsed Pucca dwellings in Bhachau taluka reached 95%, followed by Anjar and Mundra taluka with 77%. Relation of collapse ratio and human loss against epicentral distance (Figs. 4-a, 4-b) shows attenuation tendency, though they are scattered.

Damage statistics reported by Kachchh district office for town and village affairs are released by UNDP (2001) in the webpage. According to that statistics for Kachchh district, 69% of human loss occurred in urban area and 31% occurred in rural area, while urban population is less than rural. The cause of more fatality in urban area might be explained by multi-story dwellings and apartments destroyed in urban area

and streets filled with enormous amount of debris which made search and rescue more difficult. The cause should be examined with more reliable damage and casualty data.

School damage in Kachchh district is 62% of classrooms totally collapsed and 27% of those partially damaged. As for the medical facilities, 14% of 566 buildings suffered total collapse and 52% did partial damage.

Population growth from 1901 to 1991

<http://www.economywatch.com/database/population4.htm>

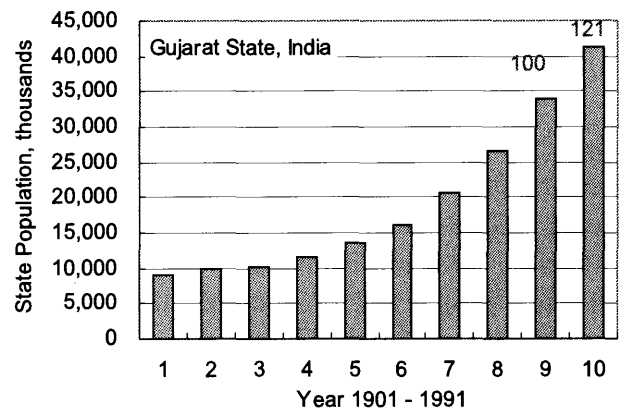


Figure 5.2. Population increase of Gujarat state from 1901 thru 1991.

Table 5.3. District-wise human loss and population

S.No. Districts	Human Death	2001 Census Population	Human Death %
1 Ahmedabad	751	5808378	0.01
2 Amreli	0	1393295	0.00
3 Anand	1	1856712	0.00
4 Banaskantha	32	2502843	0.00
5 Bharuch	9	1370104	0.00
6 Bhavnagar	4	2469264	0.00
7 Gandhinagar	8	1334731	0.00
8 Jamnagar	119	1913685	0.01
9 Junagadh	8	2448427	0.00
10 Kachchh (Bhuj)	18416	1526321	1.21
11 Kheda	0	2023354	0.00
12 Mehsana	0	1837696	0.00
13 Navsari	17	1229250	0.00
14 Patan	38	1181941	0.00
15 Porbandar	9	536854	0.00
16 Rajkot	433	3157676	0.01
17 Surat	46	4996391	0.00
18 Surendranagar	113	1515147	0.01
19 Vadodara	1	3639775	0.00
20 Sabarkantha	0	2083416	0.00
21 Valsad	0	1410680	0.00
Total:	20005	46235940	0.04

#1: 2001 population is estimated.

<http://ndmindia.nic.in/eq2001/eq2001.html>

Table 5.4. Population and human loss in the districts of Kachchh region

Taluka Name	No. of House-holds	1991 Population	Number of Dead	Dead %	Collapsed Pucca %: #3	Collapsed Kuchcha %: #3	Epic. Dist., km
BHUJ	55486	277215	4503	1.62	57	67	68
MUNDRA	13945	68652	65	0.09	77	85	85
MANDVI	27876	146034	72	0.05	49	83	118
ABDASA	17070	86402	19	0.02	22	23	152
LAKHPAT	7416	36759	2	0.01	16	8	162
NAKHATRANA	21610	116944	23	0.02	12	26	108
RAPAR	24273	150517	732	0.49	69	91	38
BHACHAU	22944	114759	7424	6.47	95	95	12
Anjar #1	32176	160640	4702	2.93	77	81	43
Gandhidham:#2	20743	104585	861	0.82	45	54	43
Total	243539	1262507	18403	1.46	59	63	

#1: ANJAR Taluka except for Gandhidham city

#2: Gandhidham city area

#3: Pucca (permanent) and Kuchcha (temporal) statistics in villages from UNDP web pag

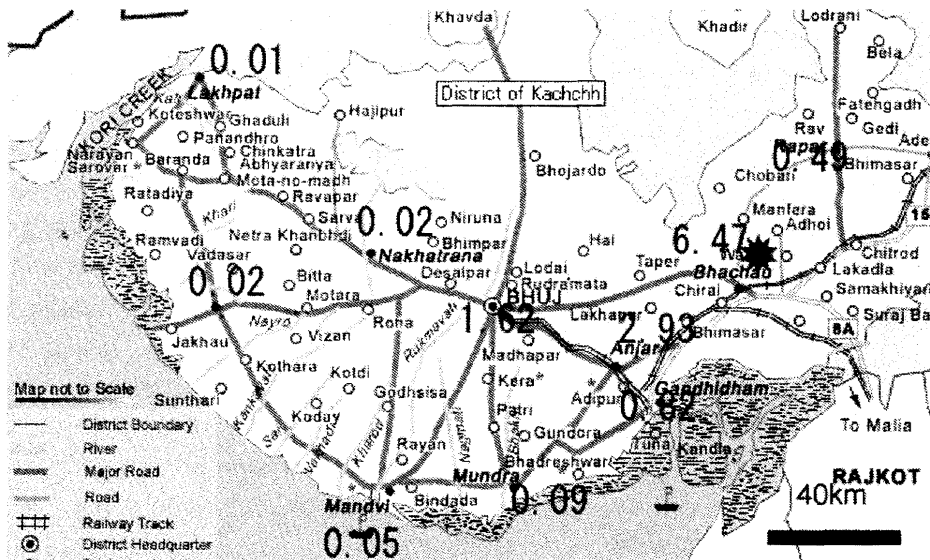


Figure 5.3. Taluka-wise fatality ratio, % in Kachchh district.

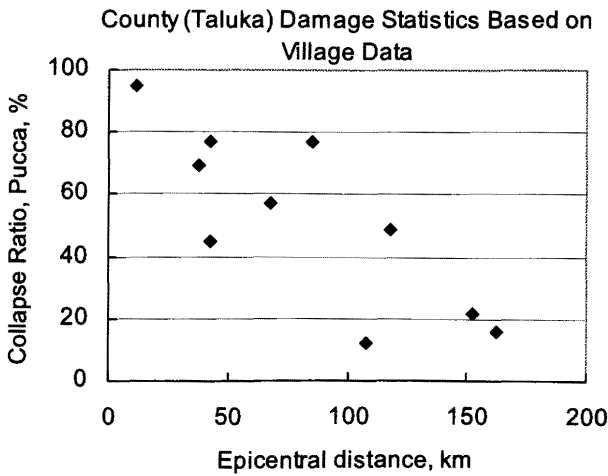


Figure 5.4-a. Collapse ratio of Pucca dwellings vs. epicentral distance.

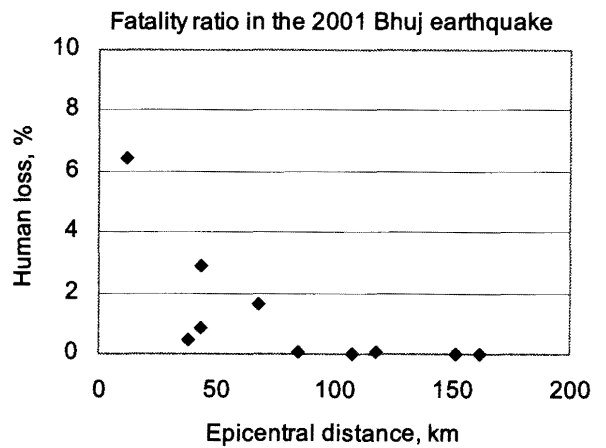


Figure 5.4-b. Human loss % vs. epicentral distance.

5. Outline of Damage Survey

(3) Emergency responses

Right after the earthquake, the Gujarat state government established a center for emergency response collecting damage data and sending SAR teams, medical teams, food, drinks and sheltering. The Gujarat state government set up the website for releasing damage and response information and asking for assistance for suffering earthquake victims in the cities and villages in the disaster area from international and national, governmental and non-governmental organizations (Gujarat State Disaster Management Authority, 2001). In the central government, crisis management center was set up at the Ministry of Agriculture (Government of India, 2001) and the work of coordination among ministries and military organization.

International Red Cross and Red Crescent Organization set up the central camp site in the college campus in Bhuj city and made coordination among various agencies (Photo 5.1). The table 5 shows collection and distribution of emergency supplies by Red Cross organization. The Relief Web site by OCHA offered up-to-date and comprehensive report from various agencies working for emergency response and relief in the disaster area and around the world.

In the disaster area, 370 dwelling units were destroyed and 1,850 thousand people lost their shelters. Partially damaged 920 thousand dwellings needed significant repair and strengthening work, so that temporal shelters for those inhabitants were additionally required. According to the Crisis Management Center of the Gujarat state government, they were making efforts to hand out building materials for simple and temporal shelter. The earthquake happened in dry season in January, and the monsoon season usually starts in June, so that provision of emergency shelters was a very difficult and outrageous task.

The State government announced the rehabilitation package plan for recovery and reconstruction of the earthquake stricken villages and towns.

- (a) Villages with collapse ratio exceeding 70%: 256 villages, among which 172 are located in Kutchch district apply. Relocation of the village is promoted and necessary infrastructure such as roads, lifelines, schools and dwellings are to be constructed. The half of the necessary expenses will be paid by the state government and the half by volunteer organization adapting a destroyed village such as private corporation, other state government, non-governmental organization of both national and international nature.
- (b) Villages, in which collapse ratio is less than 70%: Reconstruction and rehabilitation in the original site will be supported by the state government. The state also gives technical advise for repair and strengthening based on damage survey.
- (c) Disaster area located distant from the epicenter: Repairing and strengthening expenses will be assisted by the state government.
- (d) Devastated cities of Bhuj, Anjar, Bhachau, and Rapar: Owners of the residential units in apartment multi-story buildings will be assisted for repairing and strengthening according to the types of the structure.

Table 5.5. Relief items from International Red Cross

Items	Appeal target	Total received	Total distributed	Stock	Distributed in %
Blankets	210,000	230,000	228,000	2,000	109%
Tarpaulins	118,000	117,000	111,000	6,000	94%
Tents	34,038	28,600	27,600	638	81%
Kitchen Sets	60,000	60,000	41,000	19,000	68%
Water Containers	63,000	63,000	46,000	22,000	73%
BP5 (high calorie rations)	307,000	250,000	90,000	159,000	29%

Source: IFRC Date: 20 Apr 2007 Situation Rep No. 24 India/Gujarat: Earthq. Appeal No. 04/2001

5. Outline of Damage Survey

The Kachchh district is located in the most seismically active region, that is, zone V according to the 1984 seismic building code in India, however, the seismic regulations had not been enforced and resulted in collapse of many residential, commercial and industrial structures. Rural and traditional dwellings such as Kaccha and Pacca types also suffered severe devastation and caused enormous loss of human lives, housing stock and basic means of local economy to sustain community lives. During our field reconnaissance in March, temporary shelters were observed only in few and limited locations. It is important to continue the survey and observation how the lives of earthquake stricken villages and towns are to be recovered, restored with improved level of seismic safety for future earthquake risk.

References

- Government of India (2001). <http://www.ndmindia.nic.in/eq2001/eq2001.html>
- Goyal, A. et al. (2001). <http://www.civil.iitb.ernet.in/BhujEarthquake/Report1.htm>
- Grunthal, G. Editor (1998). European Macroseismic Scale 1998.
- Gujarat State Disaster Management Authority (2001). <http://www.gujaratindia.com>
- Japanese reconnaissance team (1999). Damage report of the 1999 Kocaeli, Turkey earthquake, *Natural Disaster Science*, 18, 3, pp.369-379.
- Kogakuin Univ. (2001). <http://kouzou.cc.kogakuin.ac.jp/Saigai/>
- Roorkee University (2001). <http://vision.rurk.ie.ernet.in/depts/earthquake/bhuj/>
- UNDP (2001). UNDP Bhuj site, <http://www.undpquakerehab.org/>



Photo 5.1. Campsite of the Japan Red Cross relief team (Bhuj).



Photo 5.2. Collapse of RC and masonry buildings in Bhachau center.

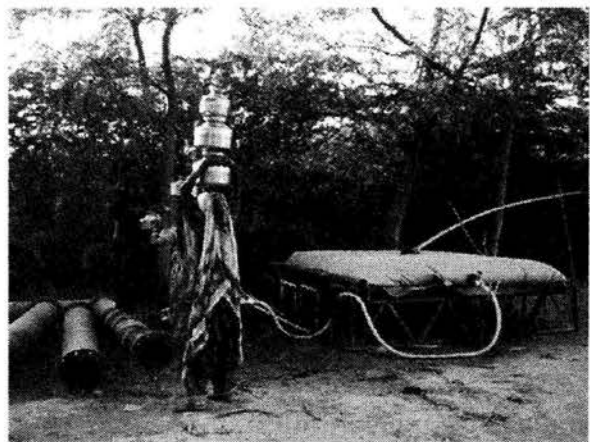


Photo 5.3. Water tank collapsed and people carry water (Berandiala).